Recovery of $Mn_{0.8}Zn_{0.2}Fe_2O_4$ from Zn–C battery: auto-combustion synthesizes, characterization, and electromagnetic properties

M. A. Gabal[1,2] · E. A. Al-Harthy[1,3] · Y. M. Al Angari[1] · A. Awad[2] · A. A. Al-Juaid[3] · A. M. Abdel-Daiem[4,5] · Abdu Saeed[4]

Abstract

$Mn_{0.8}Zn_{0.2}Fe_2O_4$ ferrites were successfully prepared via a recycling process of spent Zn–C batteries (SZCBs) using sol–gel auto-combustion techniques and different fuels, including citric acid and sucrose chitosan, gelatin, and egg-white. The cost of this recycling technology, as well as the used fuels, have both economic and environmental advantages, facilitating many promising industrial applications. XRD confirmed single-phase formation with average crystallite sizes in the range from 15 to 55 nm. The appropriate cation distribution, elucidated using structural parameters, indicated the preferential occupancy of Zn^{+2} ions only by the A-sites while Mn^{+2} and Fe^{+3} ions preferentially occupy both A and B-sites. TEM images exhibited cubically agglomerated particles with wide size distribution. VSM indicated a wide range of magnetization values (51.0–19.8 emu/g) depending on the preparation route, suggesting the impact of the fuel used. The prepared ferrite using citric acid showed the highest value, while that prepared using egg-white indicated the lowest one. The obtained coercivities indicated soft magnetic materials with a decreasing behavior by increasing sizes. The ac-conductivity indicated semiconducting characteristics with a noticeable improvement in the conductivity than that of the bulk ferrite. The temperature dependence of the ac-conductivity showed a transition from ferro- to paramagnetic by increasing temperature. The estimated Curie temperatures (T_C) indicated an improvement in the magnetic characteristics. In addition, the frequency dependence of ac-conductivity indicated a change in the conduction mechanism from the electron hopping to polaron type by increasing temperature. The very high dielectric values obtained in the order of 10^5 at low frequency warrant their application at low frequencies.

Graphical Abstract

Flow chart for the synthesis of Mn–Zn ferrite nanoparticles using spent Zn–C batteries via different sol–gel auto-combustion routes.
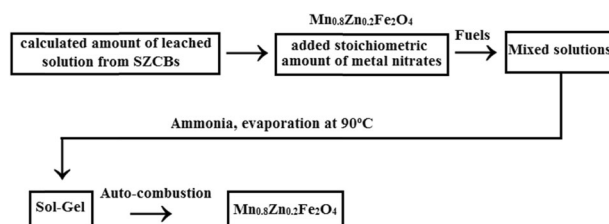
✉ M. A. Gabal
mgabalabdonada@yahoo.com

1 Chemistry Department, Faculty of Science, King Abdulaziz University, Jeddah, Saudi Arabia

2 Chemistry Department, Faculty of Science, Benha University, Benha, Egypt

3 Chemistry department, Faculty of Science, University of Jeddah, Jeddah, Saudi Arabia

4 Physics Department, Faculty of Science, King Abdulaziz University, Jeddah, Saudi Arabia

5 Physics Department, Faculty of Science, Zagazig University, Zagazig, Egypt

Highlights

- $Mn_{0.8}Zn_{0.2}Fe_2O_4$ ferrites were prepared from spent Zn-C batteries with different fuels.
- The entire ferrites were prepared using environment-friendly auto-combustion routes.
- Ferrites were characterized using XRD, TEM, and VSM.
- The different obtained properties were investigated and discussed.

1 Introduction

During the last decades, cubic-spinel ferrites gained extensive interest owing to their exceptional properties and wide applications in different fields [1]. Among cubic ferrites, manganese-zinc ferrites ($Mn–ZnFe_2O_4$), particularly, are a hot topic in scientific research due to their high permeability, low core loss, thermal stability as well as semiconducting characters [2]. In addition, as ferromagnetic materials, they are comprehensively used in various electro-magnetic applications, including core inductors, recording heads, transformers, magnetic beads, and amplifiers [3].

Zn–C batteries have been widely utilized as a small-sized portable power supply for their low cost, versatility, and ability to store energy [4]. Around the world, enormous quantities of spent Zn–C batteries (SZCBs) were discharged into the environment as solid wastes, which causes a dangerous menace to the environmental system besides losing a large amount of the main contents; Zn and Mn. Thus, considering this massive Mn and Zn reservoir concentration, the recycling of SZCBs is crucial in the management and treatment of solid waste.

The retrieval of Mn and Zn contents from SZCBs could be processed through thermal treatment [5], extraction [6], electrolysis [7], or precipitation [8]. In this case, the produced Mn and Zn elements were utilized as a raw resource for producing Mn–Zn ferrites (MZFs). Recently [9–11], the MZFs synthesis using raw materials from Zn–C batteries via reductive strong acid leaching as precursor instead of separation, extraction, or separation of metals followed by their processing represents another promising approach that gained more intensive studies. This process was found to be simple, time-saving with low cost.

In literature, many wet synthesis routes have been utilized for the MZFs preparation, including in-situ composite [12], hydrothermal [13], heat treatment [14], solvothermal [15], sol–gel [16], micro-emulsion [17], thermal decomposition of oxalates [18] and polyol route [19]. Unfortunately, these methods using expensive and often toxic chemicals and consume a long time for processing. Nowadays, auto-combustion routes are considered as one of the promising ways to prepare such ferrites [11, 20–22]. These routes are simple, low cost, and fast besides being environment friendly. The required heat for ferrites formation is provided during the occurring reaction itself; thus, no further heat processes are needed.

From all of the studies above [11–22], it was concluded that the use of different methods resulted in the different obtaining parameters such as lattice parameter, size, cation distribution, magnetization, conductivity, etc., which means gradient properties of the prepared ferrites. For this reason, in this work, a comparative study has been performed on the synthesis of $Mn_{0.8}Zn_{0.2}Fe_2O_4$ nanocrystalline ferrite via recycling Mn–Zn contents of the SZCBs through a reductive acid leaching process followed by the entire auto-combustion process using different environment-friendly fuels, including citric acid, sucrose, chitosan, gelatin and egg-white. Besides, to the best of our knowledge, no similar study was performed in this direction. In this work, the crystal phases of the prepared ferrites were evaluated using X-ray diffraction (XRD); the morphologies and chemical group function of the prepared samples were explored using transmission electron microscopy (TEM) and Fourier transform infrared spectroscopy (FT-IR), respectively. Furthermore, the magnetic properties were studied using a vibrating sample magnetometer (VSM); besides, the electrical and dielectric properties were estimated. This work could help convert the waste SZCBs into more valuable magnetic semiconducting MZFs, thus saving the environment and gaining many economic benefits.

2 Materials and methods

2.1 Materials

The A–A size SZCBs (1.5 V) of the same brand was used as obtained. Analytical reagents nitrates including $Fe(NO_3)_2 \cdot 9H_2O$, $Mn(NO_3)_2 \cdot 4H_2O$, and $Zn(NO_3)_2 \cdot 6H_2O$ (BDH) were utilized, as they are (without any more purification) to adjust the composition ratio of the entire metals to $Mn_{0.8}Zn_{0.2}Fe_2O_4$. Commercial sucrose ($C_{12}H_{22}O_{11}$), gelatin from Fluka, citric acid $C_6H_8O_7$ (BDH), and low molecular weight chitosan (BDH) were used as fuel in the auto-combustion process. Also, freshly extracted aqueous egg-white (60 ml egg-white in 40 ml distilled water) was utilized. Ammonium hydroxide (NH_4OH) (BDH) was used to adjust pH.

Table 1 Concentrations of the main analyzed elements in the Zn–C battery (mg L^{-1})

Elements	Mean
Mn	32257.7
Zn	65658.4
Fe	1018.07
Al	824.057
Pb	210.007
Ca	109.296
Co	56.8919
Cu	33.1049
Bi	23.2438
Cr	15.7997
Cd	15.6953
Ag	11.5064
V	7.1296
Ti	5.8176
As	5.2182
Hg	0.5239
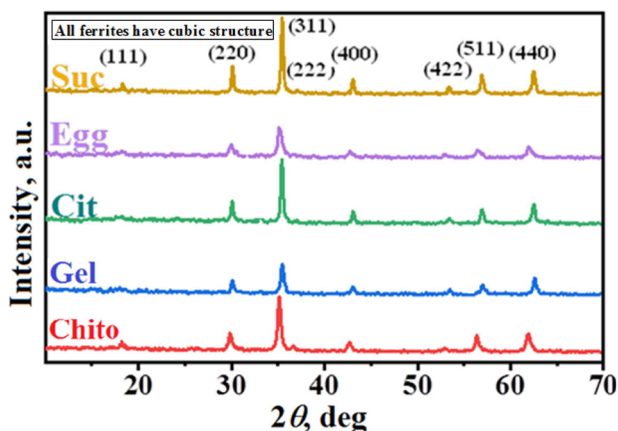
Fig. 1 XRD patterns of the prepared $Mn_{0.8}Zn_{0.2}Fe_2O_4$ ferrites prepared using different methods
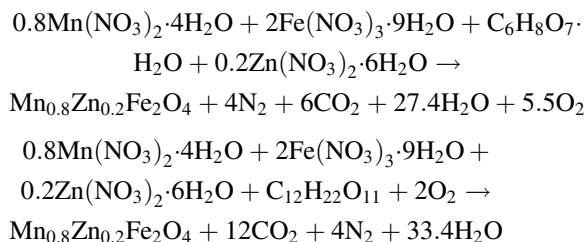
2.2 SZCBs Pretreatment and elemental analysis

The SZCBs were dismantled as following; they were manually disassembled, and the scrap, including carbon rod, copper cap, plastics, and papers, were separated. Then, the remaining contents containing high zinc and manganese compositions were crushed, ground, washed with distilled water, dried, and weighed. After that, the obtained mixture was then leached in 5 M nitric acid; HNO_3 containing 2 wt% of hydrogen peroxide (H_2O_2) under stirring at about 60 °C until complete dissolution. Finally, the filtrate was analyzed for its metal constituents by atomic absorption spectroscopy (AAS). The chemical compositions of different analyzed metals (Table 1) were previously published [11].

2.3 Synthesis and characterization of $Mn_{0.8}Zn_{0.2}Fe_2O_4$ nanoparticles

$Mn_{0.8}Zn_{0.2}Fe_2O_4$ nano-sized ferrites were prepared using the sol–gel auto-combustion technique, using different precursors including citric acid, sucrose, chitosan, gelatin, and egg-white as fuel. The details of the synthesis procedures are already discussed in our previous publications [11, 21–23]. Generally, stoichiometric amounts of zinc, manganese, and iron nitrates, equivalent to $Mn_{0.8}Zn_{0.2}Fe_2O_4$ composition, were added to the analyzed filtrate and stirred at 60 °C. The solution pH was controlled to about 7 by adding diluted ammonium solution before adding precursors, except in the case of gelatin and egg-white fuels. After aging with evaporation at about 100 °C, the obtained sticky gel was initiated to be auto-combusted with releasing dense gases and heat. The obtained powders were named following their precursors.

The representing of the auto-combustion reactions appears to be more complex in the case of egg-white, gelatin, and chitosan, being they include more than one amino acid. However, the expected auto-combustion reactions that resulted in the ferrite formation could be represented in the case of citric acid and sucrose, respectively as:

$$0.8Mn(NO_3)_2 \cdot 4H_2O + 2Fe(NO_3)_3 \cdot 9H_2O + C_6H_8O_7 \cdot$$
$$H_2O + 0.2Zn(NO_3)_2 \cdot 6H_2O \rightarrow$$
$$Mn_{0.8}Zn_{0.2}Fe_2O_4 + 4N_2 + 6CO_2 + 27.4H_2O + 5.5O_2$$

$$0.8Mn(NO_3)_2 \cdot 4H_2O + 2Fe(NO_3)_3 \cdot 9H_2O +$$
$$0.2Zn(NO_3)_2 \cdot 6H_2O + C_{12}H_{22}O_{11} + 2O_2 \rightarrow$$
$$Mn_{0.8}Zn_{0.2}Fe_2O_4 + 12CO_2 + 4N_2 + 33.4H_2O$$

The prepared $Mn_{0.8}Zn_{0.2}Fe_2O_4$ ferrites' XRD patterns were characterized using X-ray diffractometer model D8 Advance (Bruker, USA) with 40 kV, 25 mA, and CuKα irradiation; TEM images performed using the model JEOL 2010 (JEOL, Japan); FT-IR spectra were recorded using the ALPHA II (Bruker, USA) with KBr technique; hysteresis loops measured using the VSM-8600M model (Quantum Design Inc., USA) vibrating sample magnetometer operated up to a magnetic field of 15 kOe. The electrical and dielectric properties were studied on pellets using the Hioki LCR high model tester 3531 (Hioki, Japan) at temperatures up to 673 K and different frequencies.

3 Results and discussion

XRD patterns of the synthesized $Mn_{0.8}Zn_{0.2}Fe_2O_4$ ferrites using different methods are shown in Fig. 1. According to the JCPDS card No. 74-2402 and previously published works [11, 21–23], the prepared $Mn_{0.8}Zn_{0.2}Fe_2O_4$ ferrites

Table 2 Structural and electro-magnetic parameters of $Mn_{0.8}Zn_{0.2}Fe_2O_4$ ferrites prepared via different sol–gel methods

Method	Cation distribution	a_{Exp} (nm)	a_{th} (nm)	L (nm)	D_X (g cm^{-3})	D (nm)	M_S (emu/g)	M_r (emu/g)	H_C (Oe)	M_r/M_s	σ (ohm^{-1} cm^{-1})	T_C	E_f (eV)	E_p (eV)
Citric acid	$(Mn_{0.2}Zn_{0.2}Fe_{0.6})[Mn_{0.6}Fe_{1.4}]O_4$	8.3811	8.3866	15	5.25	60	51.0	8.7	175	0.17	1.0×10^{-5}	541	0.41	0.43
Sucrose	$(Mn_{0.4}Zn_{0.2}Fe_{0.4})[Mn_{0.4}Fe_{1.6}]O_4$	8.4305	8.4309	40	5.16	55	50.7	23.2	133	0.47	5.0×10^{-6}	571	0.57	0.62
Chitosan	$(Mn_{0.4}Zn_{0.2}Fe_{0.4})[Mn_{0.4}Fe_{1.6}]O_4$	8.4243	8.4309	35	5.17	39	47.1	6.0	144	0.13	2.5×10^{-6}	526	0.58	0.69
Gelatin	$(Mn_{0.4}Zn_{0.2}Fe_{0.4})[Mn_{0.4}Fe_{1.6}]O_4$	8.4466	8.4309	23	5.13	50	26.0	1.9	87	0.07	2.0×10^{-6}	588	0.53	0.76
Egg-white	$(Mn_{0.2}Zn_{0.2}Fe_{0.6})[Mn_{0.6}Fe_{1.4}]O_4$	8.3800	8.3866	55	5.27	48	19.8	2.2	133	0.11	2.8×10^{-6}	555	0.70	0.95

possess a cubic spinel structure. The crystallite size (L), lattice parameter (a_{Exp}), X-ray density (D_x), and cation distributions are listed in Table 2. XRD pattern of the sample prepared using chitosan as fuel and measured for the first time indicated a similar trend as those prepared using other methods. In addition, the absence of any secondary diffraction peaks indicated the formation of the complete ferrite without the need for further calcination.

As previously described in [11, 21, 22], an appropriate cation distribution was elucidated using the calculated lattice parameters (a_{th}) and the preferential occupancy of the entire cations (Mn^{+2}, Zn^{+2}, and Fe^{+3}) in different crystalline lattices (A and B-sites). Generally, the calculated lattice parameters were in excellent agreement with the experimentally obtained ones (Table 2). The cation distribution of the prepared ferrite using the chitosan route was elucidated by comparing its experimental lattice parameters with those reported for other ferrites.

Generally, the estimated cation distribution of the different studied ferrites (Table 2) indicated the preferential occupancy of Zn^{+2} ions only by the tetrahedral A-sites. In contrast, the Mn^{+2} ions preferentially occupy both A and B-sites. In addition, the prepared ferrites using sucrose, chitosan, and gelatin methods showed similar cation distribution as $(Zn_{0.2}Mn_{0.4}Fe_{0.4})[Mn_{0.4}Fe_{1.6}]O_4$, while others prepared through citric acid and egg-white methods exhibited less Mn^{+2} ions at tetrahedral sites: $(Zn_{0.2}Mn_{0.2}Fe_{0.6})[Mn_{0.6}Fe_{1.4}]O_4$.

The calculated X-ray densities of the ferrites prepared via citric acid and egg-white methods appeared to be higher than those calculated by other methods depending on their lower volume (a_{Exp}^3). The average calculated crystallite sizes (L) exhibited nano-crystalline characteristics of all the studied ferrites ranging from 15 to 55 nm. The ferrite prepared using citric acid indicated the smaller sizes, while the prepared using egg white exhibited the higher ones.

TEM images (Fig. 2) confirmed the nano-crystalline characteristics of the studied ferrites. The images captured by TEM showed cubic conglomerated particles with wide size distribution. The averages of the particle size are summarized in Table 2. The reported values generally exhibited higher values than calculated crystallite sizes via XRD, which may be attributed to the agglomeration phenomena. This agglomeration could arise mainly from the permanent magnetization of particles exerting a permanent magnetic moment commensurate to their volume [24] or due to the slow particle's growth during the synthesis process [25].

The prepared ferrite using the egg-white method (Fig. 2b) showed the least agglomerated one compared to that prepared using the citric acid route (Fig. 2a), which exhibited the highest agglomeration. This behavior could be easily discussed through their related magnetic properties, as will be presented later.
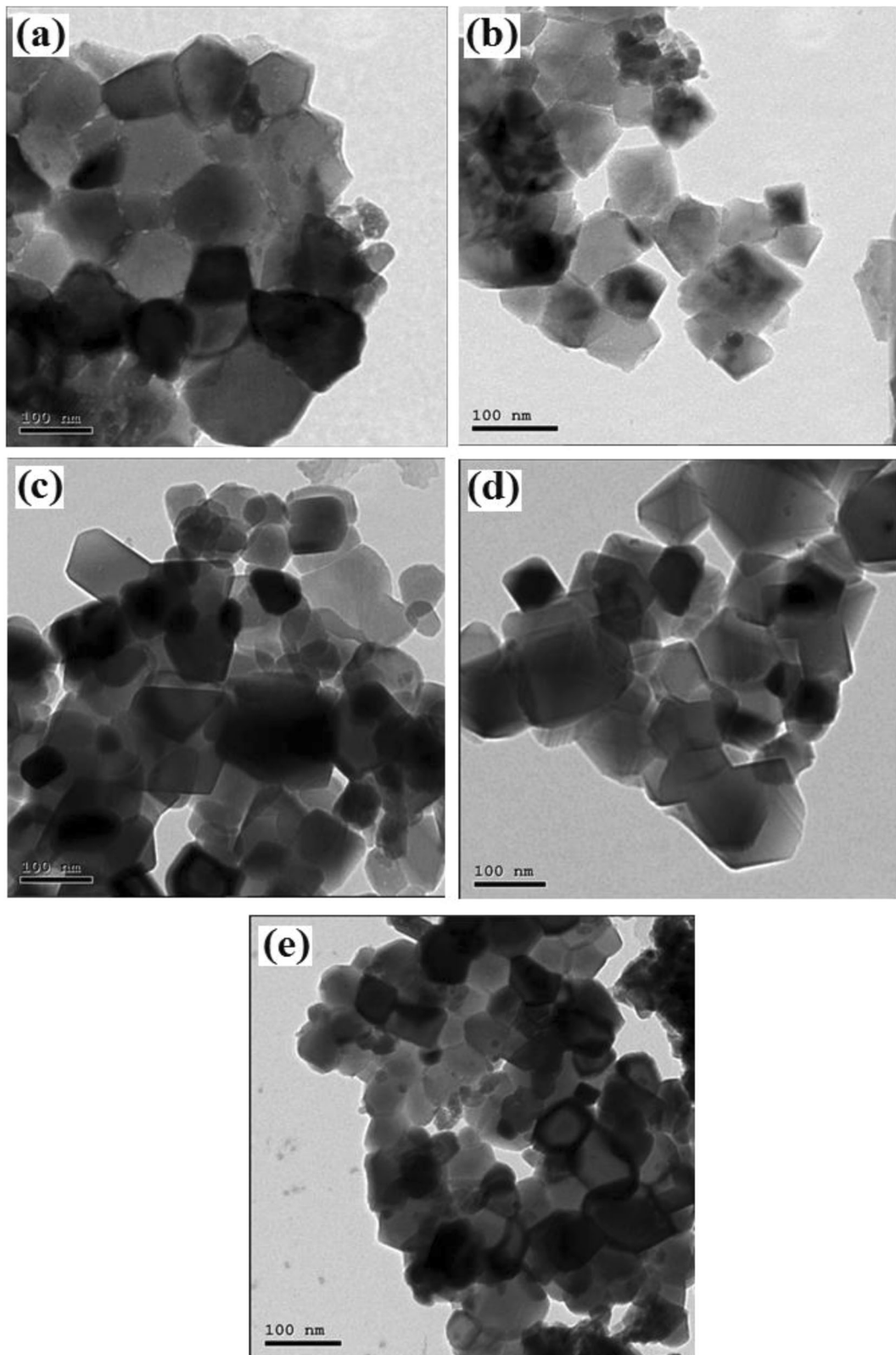
Fig. 2 TEM images of the prepared $Mn_{0.8}Zn_{0.2}Fe_2O_4$ ferrites prepared using different fuels. (a) Citrate, (b) egg-white, (c) gelatin, (d) sucrose and € chitosan. Scale bar = 100 nm
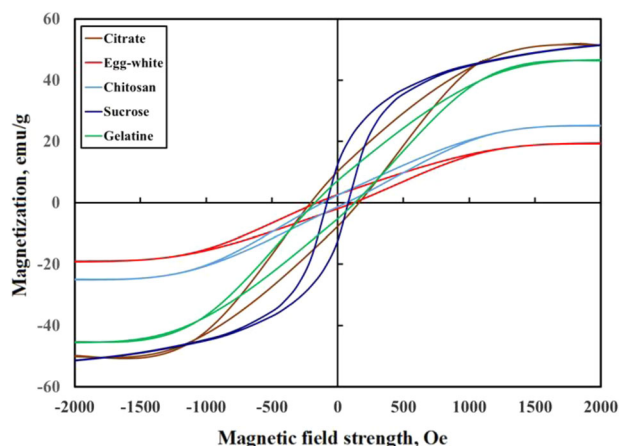
Fig. 3 Hysteresis loops for the prepared $Mn_{0.8}Zn_{0.2}Fe_2O_4$ ferrites prepared using different methods

The hysteresis loops of $Mn_{0.8}Zn_{0.2}Fe_2O_4$ ferrites prepared using different methods are exhibited in Fig. 3. The different estimated magnetic parameters are summarized in Table 2. The studied samples indicated ferromagnetic behavior with harmonic saturation magnetization values (M_s) ranging between 51.0 and 19.8 emu/g. The prepared ferrite using citric acid showed the highest value while using the egg-white displayed the lowest one. This obtained wide range of magnetization could achieve a variety of applications according to the needed magnetic properties.

Generally, the obtained magnetization from all the prepared ferrites appeared to be lower than that reported for the bulk $Mn_{0.8}Zn_{0.2}Fe_2O_4$ (83.82 emu/g) [26]. In addition, the obtained magnetization values seemed to have lower values than those already reported in the literature for $Mn_{0.8}Zn_{0.2}Fe_2O_4$ prepared using different sol–gel methods [27–29]. This difference could be attributed to the source of the used chemicals (the spent Zn–C battery), size effect, disordered spins within a surface layer, or simply to the expected difference in the cation distribution [30, 31].

A comparative study for the obtained magnetization values (Table 2) showed different values depending on the preparation route, indicating the impact of the fuel used during the auto-combustion process. The obvious difference in the magnetization values despite similar estimated cation distribution, for example, in the case of ferrites prepared by sucrose, chitosan, and gelatin methods (Table 2), showed that the cation distribution could be not the only agent that influences the magnetization. Still, other agents such as size, disordered spins, defects, surface effect, or strains must also be taken into consideration. Also, it could be observed that the larger the crystallinity, the greater the magnetization value, as can be seen from XRD patterns (Fig. 1) of ferrites prepared using citric acid, sucrose, and chitosan. Similar behavior was reported in the literature for MZFs prepared by co-precipitation and ball-milled routes [32, 33].

The obtained coercivity values (Table 2) indicated soft magnetic materials, which means ease in magnetization and demagnetization effects. The prepared ferrite through the chitosan method showed the least coercivity (87 Oe) while that prepared via the citric acid route exhibited the larger one (175 Oe). The coercivity is well known to be a micro-structure property [34], since it has proportional relations with size, defects, strains, surface effect, etc. From a close look at Table 2, one can observe the coercivity dependence on particle sizes through comparing coercivities (H_c) and sizes (D) of ferrites prepared via citric acid and chitosan methods. It is clear that the coercivity showed a decreasing behavior with increasing size. Generally, the coercivities recorded in this work showed higher values than those in the published work for $Mn_{0.8}Zn_{0.2}Fe_2O_4$ ferrite prepared via auto-combustion routes [35, 36].

Overall, the obtained squareness ratios (M_r/M_s) (where M_r refers to remanent magnetization, i.e., magnetization at zero magnetic field strength) as reported in Table 2, indicated according to the literature [12, 37, 38], that the presently prepared ferrites are of multi-domains since their values are lower than 0.5. Accordingly, the domain wall could move smoother under the magnetic field, and the main magnetization mechanism will be the reversible domain wall motion [12, 39].

The natural logarithms of the electrical conductivities ($\ln\sigma$) versus reciprocal absolute temperature ($1000/T$) were represented in Fig. 4; they exhibited semiconducting characteristics for all studied ferrites, where the electrical conductivity displayed a progressive increase while increasing temperature. The noticeable diminution in the electrical conductivity values at initial temperatures could be referred to, as previously described in our publication [40], as the evaporation of physically adsorbed water formed during samples' preparation for conductivity measurements. The release of this water (behaving as an electron donor) by increasing temperature decreases the conductivity up to temperatures varying with respect to the studied ferrite between 350 and 390 K (Fig. 4).

At the applied frequency of 500 kHz, the conductivity values were estimated at the end of water evaporation to assure that the measured conductivity was only attributed to the entire ferrite without any water content, the measured values were summarized in Table 2. The reported values indicated a narrow range of conductivities in which the ferrite prepared using the citric acid method showed the highest value, and that prepared using gelatin showed the least one. Generally, the obtained values in the present work indicated an obvious improvement in the conductivity than that of the bulk polycrystalline $Mn_{0.8}Zn_{0.2}Fe_2O_4$ prepared using the conventional ceramic method (7.73×10^{-8} ohm^{-1} cm^{-1}) [41].

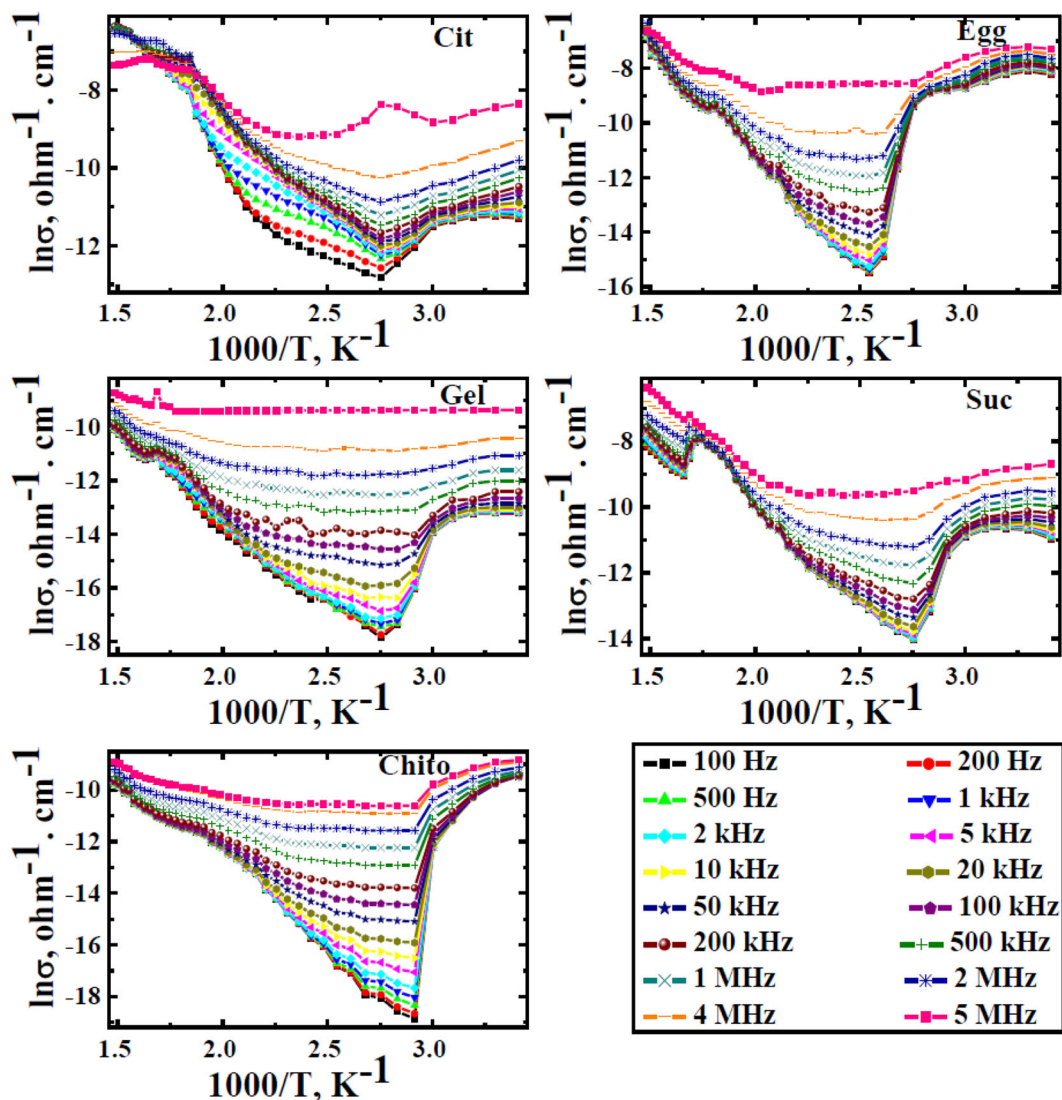The improvement in the conductivity values could be discussed in the view of electron hopping between

Fig. 4 $\ln\sigma$ vs. $1000/T$ as a function of frequency for the prepared $Mn_{0.8}Zn_{0.2}Fe_2O_4$ ferrites prepared using different methods

mixed-valence ions of iron and manganese content. Firstly, Iron goes as Fe^{3+}, while manganese goes as Mn^{2+} in the entire spinel lattice. The heat generated due to the auto-combustion reactions during ferrites formation may lead to the evaporation of some Zn^{+2} ions from the spinel lattice, resulting in non-stoichiometry in the charge balance [42]. Besides, the formation of Mn^{+3} into the lattice at the expense of the lost Zn^{+2} ions increases this charge imbalance. Some of the Fe^{+3} ions could be converted into Fe^{+2} ions to overcome this imbalance and retains charge neutrality. Thus, in such ferrites type, the presence of Fe^{2+} and Mn^{3+} ions could increase the hopping between $Fe^{2+} \leftrightarrow Fe^{3+}$ and $Mn^{3+} \leftrightarrow Mn^{2+}$ ions resulting in increasing conductivity.

In the ascending part of the conductivity vs. temperature (Fig. 4), the change in the slope resulted in the appearance of two distinct ascending regions given the names; low temperature and high-temperature regions,

respectively. This change in the slope by increasing temperature was assigned by Ravinder and Latha [41] to the magnetic transition from ferromagnetic at low-temperature range to paramagnetic at high-temperature range. The temperature at which such transition occurred is called Curie temperature (T_C); it agreed well with that estimated for MZFs [41]. The listed values of T_C (Table 2) indicated obviously higher values than that reported for bulk $Mn_{0.8}Zn_{0.2}Fe_2O_4$ (521 K) indicating, an improvement in the magnetic characteristics.

The activation energies in the ferromagnetic (E_f) and paramagnetic (E_p) regions were obtained using Arrhenius plots of the relation; $\sigma = \sigma_0 \exp -(E_a/KT)$; they were tabulated in Table 2. It is clear from this table that the estimated activation energies in the paramagnetic regions showed higher values than that those in the ferromagnetic regions, which agreed well with Irkhin and Turov's
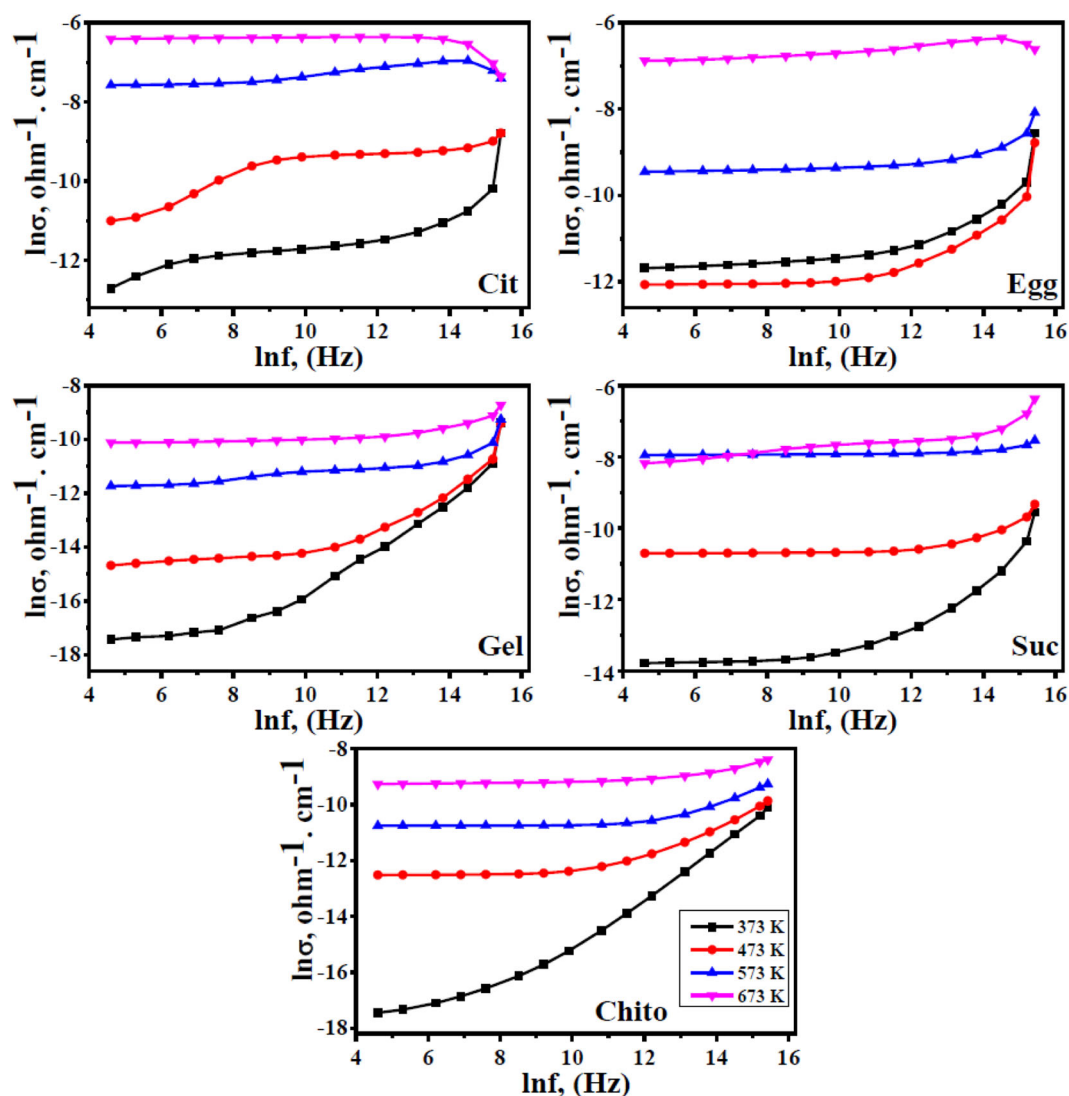
Fig. 5 $\ln\sigma$ vs. frequency as a function of temperatures for the prepared $Mn_{0.8}Zn_{0.2}Fe_2O_4$ ferrites prepared using different methods

theory [43] and reported values for other similar mixed ferrites [41, 44].

Figure 5 illustrates the variation in the measured conductivity against applied frequencies at different absolute temperatures for the studied ferrites. From the figure, an increase in the electrical conductivity could be observed with increasing the applied frequencies at low temperatures, which changed to frequency-independent behaviors at high temperatures. In this category, the applied frequency seemed to be a pumping force that plays an important role in facilitating the liberation of the trapped charges and smoothing their switching between localized states [40]. The created lattice vibrations start dispersing the charge carriers at the high temperatures range, leading to overcomes the frequencies' effects. According to the previous studies on similar ferrite systems [40, 45–47], the noticed behavior in the electrical conductivity vs. applied frequencies as different temperatures could be referred to as the conduction mechanism gets changed. The gradual increase in conductivity vs. frequency at lower temperatures could result from the electron hopping, while that almost linear behavior at higher temperatures could be assigned to the polaron type conduction.

The ferrites' dielectric properties depend mainly on structural factors [48]. The plots of both dielectric constants and dielectric loss vs. applied frequencies at different absolute temperatures of $Mn_{0.8}Zn_{0.2}Fe_2O_4$ ferrites prepared using different methods were exhibited in Figs. 6 and 7, respectively. From the figures, it is well clear that the dielectric values are both frequency and temperature-dependent. By increasing frequency, the dielectric values showed an exponential decay while gradually increase with increasing temperature. In addition, they showed frequency dependence at lower frequencies while, at higher ones a
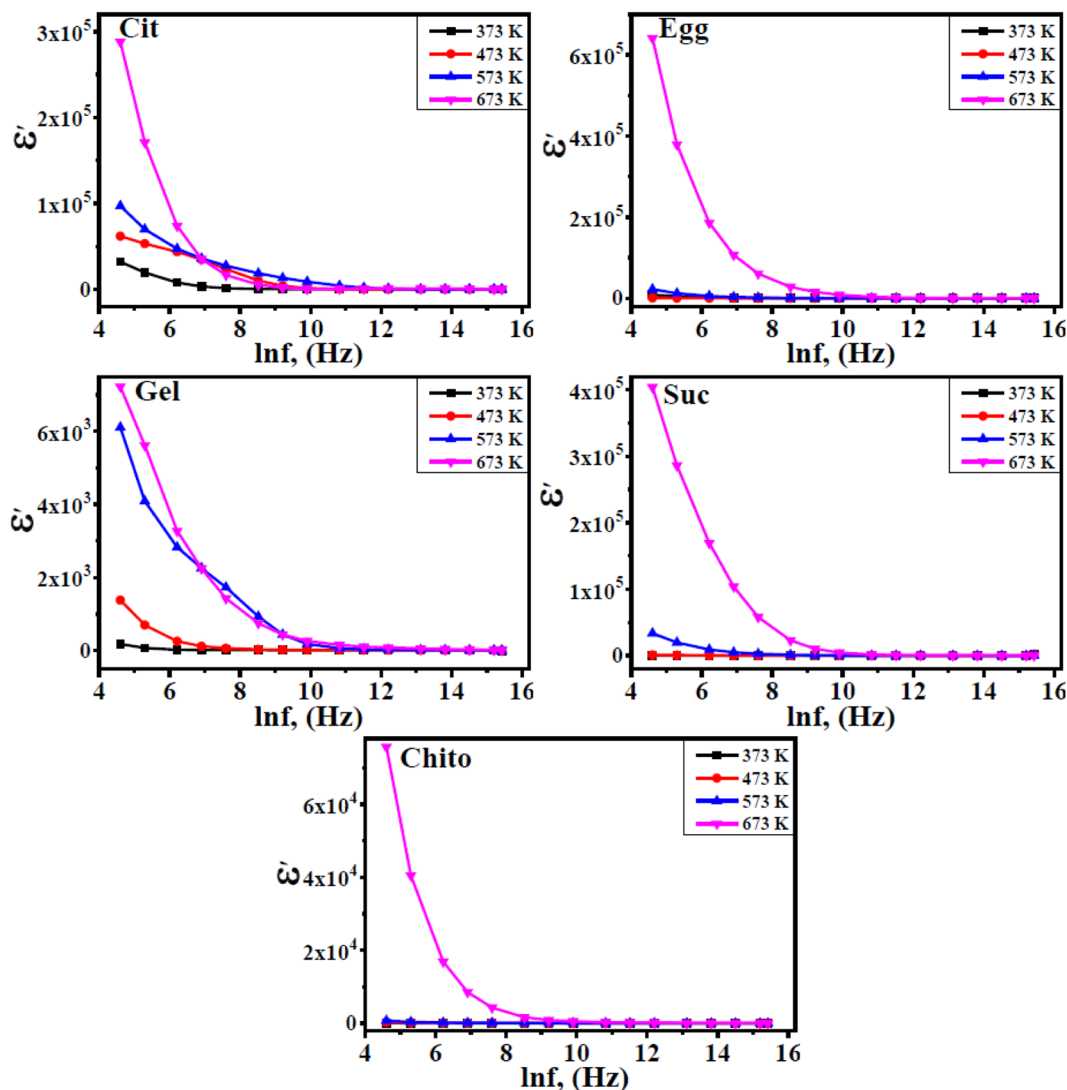
Fig. 6 Dielectric constant (ε') vs. frequency as a function of temperature for the prepared $Mn_{0.8}Zn_{0.2}Fe_2O_4$ ferrites prepared using different methods

nearly constant values. The high values of the dielectric constants obtained at lower frequencies agreed well with that reported for MZFs [48].

The dielectric parameters can be explained according to the Maxwell–Wagner model in the line of Koop's phenomenological hypothesis [49]. At low frequencies, the interfacial polarization could be increased on the applied electric field due to the piling of hopping electrons at poor conducting grain boundaries. Therefore, the more the hopping between $Fe^{2+} \leftrightarrow Fe^{3+}$ and $Mn^{3+} \leftrightarrow Mn^{2+}$ ions, the more the interfacial polarization is due to the smooth electron transfer, causing higher values of the dielectric constant [50]. The dipoles cannot follow up the frequency variations while maximizing the frequencies, causing decreases in the dielectric values. At high frequencies, the atomic and electronic polarizations could be the main factors, and hence the dielectric parameters are almost independent of frequency and become steady [48].

The very high dielectric values obtained in the order of 10^5 at low frequency (Fig. 6) could be resulted by space charge polarization, which can reduce the penetrating depth of the electromagnetic radiation by increasing the skin effect and thus warrant their application at low frequencies [48, 51].

4 Conclusions

Nano-crystalline $Mn_{0.8}Zn_{0.2}Fe_2O_4$ ferrites have been successfully synthesized using SZCBs via different sol–gel auto-combustion methods. XRD results confirmed a single-phase structure without the need for any further calcination. An appropriate cation distribution was elucidated using structural parameters. The obtained averages crystallite sizes (L) were in the range of 15 to 55 nm. TEM images showed cubic
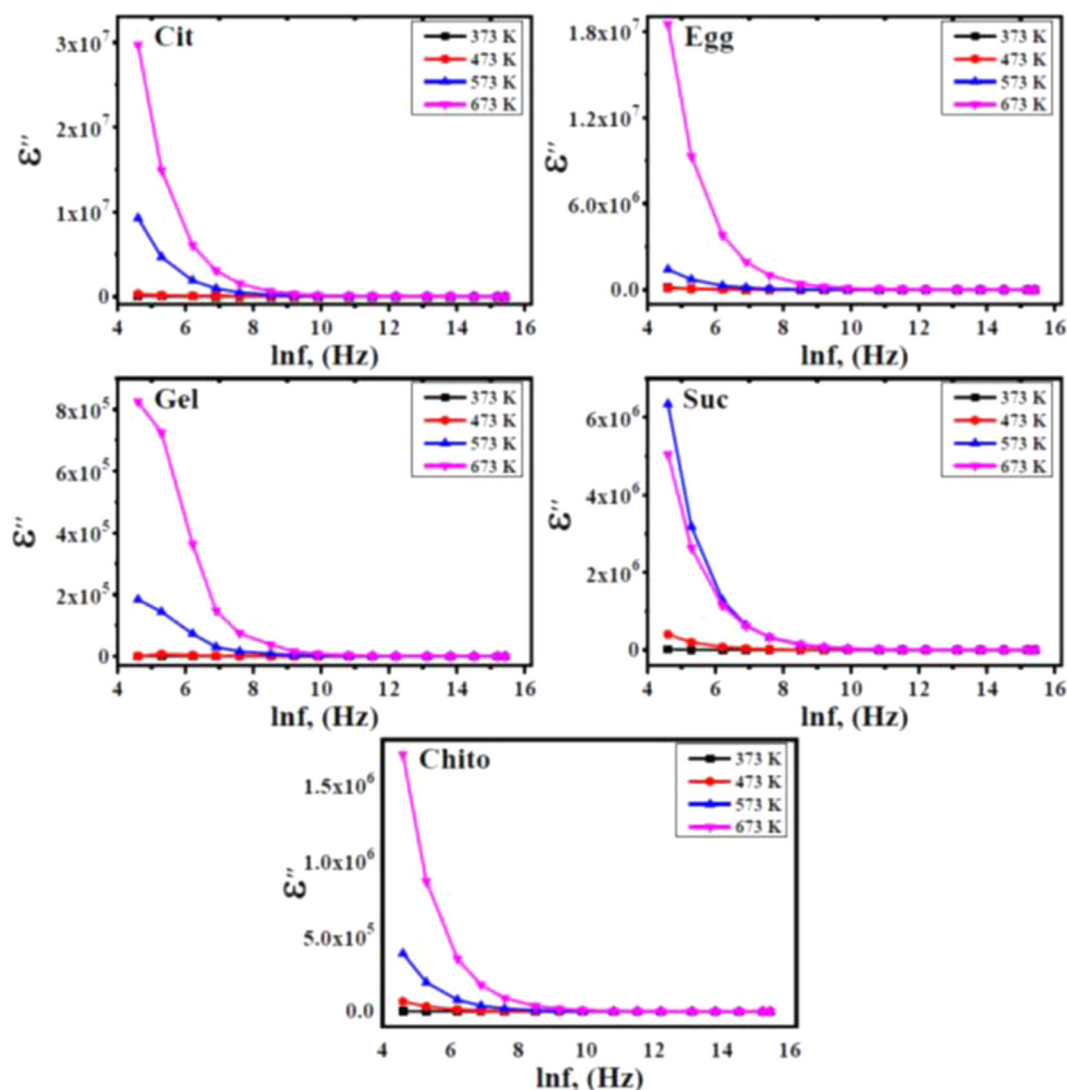
Fig. 7 Dielectric loss (ε'') vs. frequency as a function of temperatures for the prepared $Mn_{0.8}Zn_{0.2}Fe_2O_4$ ferrites prepared using different methods

agglomerated particles with wide size distribution. VSM measurements indicated saturation magnetization values (M_s) ranging between 51.0 and 19.8 emu/g, which are lower than that reported for bulk $Mn_{0.8}Zn_{0.2}Fe_2O_4$ ferrite (83.82 emu/g) and those other prepared via sol–gel routes already reported in the literature. The prepared ferrite using citric acid showed the highest value, while that prepared using the egg-white method indicated the lowest one. On the other hand, the coercivities obtained are higher than those reported in the literature. The electrical conductivity investigations indicated semiconducting behaviors with an obvious improvement in the conductivity than that of the bulk polycrystalline $Mn_{0.8}Zn_{0.2}Fe_2O_4$ (7.73×10^{-8} ohm^{-1} cm^{-1}). The measurements also showed a ferro- to paramagnetic transition with higher values of Curie temperatures (T_C) than that reported for bulk $Mn_{0.8}Zn_{0.2}Fe_2O_4$ (521 K), indicating an improvement in the magnetic characteristics. The very high dielectric

values obtained in the order of 10^5 at low frequency warrant their application at low frequencies.

Availability of data and material

Data and materials will be available on demand.

Compliance with ethical standards

References

1. Goldman A (2006) Modern ferrite technology. Springer, New York, NY

2. Angermann A, Topfer J (2011) Synthesis of nano-crystalline Mn–Zn ferrite powders through thermolysis of mixed oxalates. Ceram Int 37:995–1002

3. Qu J, Feng Y, Zhang Q, Cong Q, Luo C, Yuan X (2015) A new insight of recycling of spent Zn–Mn alkaline batteries: synthesis of $Zn_xMn_{1-x}O$ nanoparticles and solar light driven photocatalytic degradation of bisphenol A using them. J Alloy Compds 622:703–707

4. Wang J, Tian B, Niu Z, Qi S, Bao Y, Xin B (2019) Synthesis of nano-sized Zn–Mn ferrite from the resulting bioleachate of obsolete Zn-Mn batteries at a high pulp density of 5.0% enhanced by the added Fe^{3+}. J Clean Prod 229:299–307

5. Belardi G, Lavecchia R, Medici F, Piga L (2012) Thermal treatment for recovery of manganese and zinc from zinc-carbon and alkaline spent batteries. Waste Manag 32:1945–1950

6. Akash D, Kamal K, Parveen K, Pawan K, Amit LS, Bina G, Lalit MB (2011) Recovery of pure ZnO nanoparticles from spent $Zn–MnO_2$ alkaline batteries. Environ Sci Technol 45:10551–10556

7. Racz R, Ilea P (2013) Electrolytic recovery of Mn_3O_4 and Zn from sulphuric acid leach liquors of spent zincecarboneMnO_2 battery powder. Hydrometallurgy 139:116–123

8. Leao QC, Carlos AJ, Augusto VC, Gante V, Luiz MJ (2014) Recovery of manganese and zinc via sequential precipitation from spent zinc-MnO_2 dry cells after fusion with potassium hydrogen sulfate. J Power Sources 248:596–603

9. Peng CH, Bai BS, Chen YF (2008) Study on the preparation of Mn–Zn soft magnetic ferrite powders from waste Zn–Mn dry batteries. Waste Manag 28:326–332

10. Kim TH, Senanayake G, Kang JG, Sohn JS, Rhee KI, Lee SW, Shin SM (2009) Reductive acid leaching of spent zinc-carbon batteries and oxidative precipitation of Mn–Zn ferrite nanoparticles. Hydrometallurgy 96:154–158

11. Gabal MA, Al-luhaibi RS, Al-Angari YM (2012) Mn–Zn nano-crystalline ferrites synthesized from spent Zn–C batteries using novel gelatin method. J Hazard Mater 246:227–233

12. Xu Z, Fan J, Han Y, Liu T, Zhang H, Song K, Zhang C (2019) Preparation and characterization of Mn–Zn ferrites via nano-in-situ composite method. Sol Stat Sci 98:106006

13. Shebla A, Hassan AA, Salama DM, Abd El-Aziz ME, Abd Elwahed MSA (2020) Template-free microwave-assisted hydrothermal synthesis of manganes-zinc ferrite as a nanofertilizer for squash plant (Cucurbita pepo L). Heliyon. e03596

14. Al-Hada NM, Kamari HM, Shaari Abdul H, Saion E (2019) Fabrication and characterization of manganese–zinc ferrite nanoparticles produced utilizing heat treatment technique. Results Phys 12:1821–1825

15. Lin Z, Xiaoling P, Xinqing W, Hongliang G, Jing Z, Yunwei X (2015) Preparation and characterization of manganese-zinc ferrites by a solvothermal method. Rare Met Mater Eng 44:1062–1066

16. Limin D, Zhidong H, Yaoming Z, Ze W, Xianyou Z (2006) Preparation and sinterability of Mn–Zn ferrite powders by sol-gel method. J Rare Earths 24:54–56

17. Mathew DS, Juang RS (2007) An overview of the structure and magnetism of spinel ferrite nanoparticles and their synthesis in microemulsions. Chem Eng J 129:51–65

18. Angermann A, Topfer J (2011) Synthesis of nano-crystalline Mn–Zn ferrite powders through thermolysis of mixed oxalates. Ceram Int 37:995–1002

19. Topfer J, Angermann A (2011) Nanocrystalline magnetite and Mn–Zn ferrite particles via the polyol process: Synthesis and magnetic properties. Mater Chem Phys 129:337–342

20. Gabal MA, Al-Luhaibi RS, Al Angari YM (2013) Effect of Zn-substitution on the structural and magnetic properties of Mn–Zn ferrites synthesized from spent Zn–C batteries. J Magn Magn Mater 348:107–112

21. Gabal MA, Al-luhaibi RS, Al Angari YM (2014) Recycling spent zinc-carbon batteries through synthesizing nano-crystalline Mn–Zn ferrites. Powder Technol 256:32–37

22. Gabal MA, Al-Harthy EA, Al Angari YM, Abdel Salam M, Asiri AM (2016) Synthesis, characterization and magnetic properties of MWCNTs decorated with Zn-substituted $MnFe_2O_4$ nanoparticles using waste batteries extract. J Magn Magn Mater 407:175–181

23. Al Angari YM (2018) Electro-magnetic properties of nano-crystalline Mn–Zn ferrite synthesized from spent Zn–C battery via Egg-white route. Int J Electrochem Sci 13:12331–12339

24. Manova E, Kunev B, Paneva D, Mitov I, Petrov L, Estournes C, D'Orleans C, Rehspringer JL, Kurmoo M (2004) Mechano-synthesis, characterization, and magnetic properties of nano-particles of cobalt ferrite, $CoFe_2O_4$. Chem Mater 16:5689–5696

25. Jahanbin T, Hashim M, Mantori K (2010) Comparative studies on the structure and electro-magnetic properties of Ni–Zn ferrites prepared via co-precipitation and conventional ceramic processing routes. J Magn Magn Mater 322:2684–2689

26. Dasgupta S, Das J, Eckert J, Manna I (2006) Influence of environment and grain size on magnetic properties of nano-crystalline Mn–Zn ferrite. J Magn Magn Mater 306:9–15

27. Hou X, Feng J, Liu X, Ren Y, Fan Z, Zhang M (2011) Magnetic and high rate adsorption properties of porous $Mn_{1-x}Zn_xFe_2O_4$ ($0 \leq x \leq 0.8$) adsorbents. J Colloid Interface Sci 353:524–529

28. Gimenes R, Baldissera MR, da Silva MRA, da Silveira CA, Soares DAW, Perazolli LA, da Silva MR, Zaghete MA (2012) Structural and magnetic characterization of $Mn_xZn_{1-x}Fe_2O_4$ ($x = 0.2; 0.35; 0.65; 0.8; 1.0$) ferrites obtained by the citrate precursor method. Ceram Int 38:741–746

29. Syue M, Wei F, Chou C, Fu C (2011) Magnetic, dielectric, and complex impedance properties of nano-crystalline Mn–Zn ferrites prepared by novel combustion method. Thin Solid Films 519:8303–8306

30. Kanade KG, Amalnerkar DP, Potdar HS, Kale BB (2009) Nanocrystalline Mn–Zn–ferrite by novel oxalato-hydrazinated complex method. Mater Chem Phys 117:187–191

31. Angermann A, Topfer J, da Silva KL, Becker KD (2010) Nano-crystalline Mn–Zn ferrites from mixed oxalates: synthesis, stability and magnetic properties. J Alloy Compds 508:433–439

32. Meng YY, Liu ZW, Dai HC, Yu HY, Zeng DC, Shukla S, Ramanujan RV (2012) Structure and magnetic properties of Mn$(Zn)Fe_{2-x}RE_xO_4$ ferrite nano-powders synthesized by co-precipitation and refluxing method. Powder Techn 229:270–275

33. Zheng ZG, Zhong XC, Zhang YH, Yu HY, Zeng DC (2008) Synthesis, structure and magnetic properties of nano-crystalline $Zn_xMn_{1-x}Fe_2O_4$ prepared by ball milling. J Alloy Compds 466:377–382

34. Baba AA, Adekola AF, Bale RB (2009) Development of a combined pyro- and hydro-metallurgical route to treat spent zinc-carbon batteries. J Hazard Mater 171:838–844

35. Nalbandian L, Delimitis A, Zaspalis VT, Deliyanni EA, Bakoyannakis DN, Peleka EN (2008) Hydrothermally prepared nano-crystalline Mn–Zn ferrites: Synthesis and characterization. Microporous Mesoporous Mater 114:465–473

36. Wu S, Sun A, Xu W, Zhang Q, Zhai F, Logan P, Volinsky AA (2012) Iron-based soft magnetic composites with Mn–Zn ferrite nanoparticles coating obtained by sol–gel method. J Magn Magn Mater 324:3899–3905

37. Kagdi AR, Solanki NP, Carvalho FE, Meena SS, Bhatt P, Pullar RC, Jotania RB (2018) Influence of Mg substitution on structural, magnetic and dielectric properties of X-type barium zinc hex-aferrites $Ba_2Zn_{2-x}Mg_xFe_{28}O_{46}$. J Alloy Compd 741:377–391

38. Chauhan CC, Kagdi AR, Jotania RB, Upadhyay A, Sandhu CS, Shirsath SE, Meena SS (2018) Structural, magnetic and dielectric properties of Co-Zr substituted M-type calcium hexagonal ferrite nanoparticles in the presence of α-Fe_2O_3 phase. Ceram Int 44:17812–17823

39. Yu Z (2009) Research on several key technologies of high conductivity MnZn Ferrite. University of Electronic Science and Technology

40. Gabal MA, Al-Juaid AA (2020) Cr-substitution effect on structural and electro-magnetic properties of Mg-Ni ferrite synthesized via sucrose auto-combustion method. J Alloy Compd 813:152250

41. Ravinder D, Latha K (1994) Electrical conductivity of Mn–Zn ferrites. J Appl Phys 75:6118

42. Singh AK, Verma A, Thakur OP, Prakash C, Goel TC, Mendiratta RG (2003) Electrical and magnetic properties of Mn–Ni–Zn ferrites processed by citrate precursor method. Mater Lett 57:1040–1044

43. Irkhin IP, Turov EA (1959) Magnetic resonance in rhombohedral weak ferromagnetics. Sov Phys JETP 33:673

44. Ravinder D, Reddy KS, Mahesh P, Rao TB, Venudhar YC (2004) Electrical conductivity of chromium substituted copper ferrites. J Alloy Compds 370:L17–L22

45. Gabal MA, Al Angari YM, Zaki HM (2014) Structural, magnetic and electrical characterization of Mg–Ni nano-crystalline ferrites prepared through egg-white precursor. J Magn Magn Mater 363:6–12

46. Gabal MA, Al-Juaid AA, Al-Rashed SM, Hussein MA, Al-Marzouki F (2017) PSynthesis characterization and electro-magnetic properties of Zn-substituted $CoFe_2O_4$ via sucrose assisted combustion route. J Magn Magn Mater 426:670–679

47. Fu Y-P, Hu S-H (2010) Electrical and magnetic properties of magnesium-substituted lithium ferrite. Ceram Int 36:1311–1317

48. Verma A, Chatterjee R (2006) Effect of zinc concentration on the structural, electrical and magnetic properties of mixed Mn–Zn and Ni–Zn ferrites synthesized by the citrate precursor technique. J Magn Magn Mater 306:313–320

49. Junaid M, Khan MZ, Akhtar MZ, Hussain A, Warsi MF (2019) Impact of indium substitution on dielectric and magnetic properties of $Cu_{0.5}Ni_{0.5}Fe_{2-x}O4$ ferrite materials. Ceram Int 45:13431–13437

50. Deeptya M, Srinivasa CH, Kumar ER, Ramesh PN, Mohan NK, Meena SS, Prajapat CL, Verma A, Sastry DL (2020) Evaluation of structural and dielectric properties of Mn^{2+}-substituted Zn spinel ferrite nanoparticles for gas sensor applications. Sens Actuators B Chem 316:128127

51. Van Uitert LG (1956) Dielectric properties of and conductivity in ferrites. Proc IRE 44:1294–1303